Surface Science 603 (2009) 1203–1211

Contents lists available at ScienceDirect

Surface Science

journal homepage: www.elsevier.com/locate/susc

Selective surface chemistry of allyl alcohol and allyl aldehyde on Si(100)2×1: Competition of [2 + 2] C=C cycloaddition with O–H dissociation and with [2 + 2] C=O cycloaddition in bifunctional molecules

Maryam Ebrahimi, K.T. Leung *

WATLab, and Department of Chemistry, University of Waterloo, Waterloo, Ontario N2L 3G1, Canada

ARTICLE INFO

Article history:
Received 12 January 2009
Accepted for publication 3 March 2009
Available online 13 March 2009

Keywords:
Organic functionalization
Selectivity
Allyl alcohol
Allyl aldehyde
Bifunctional molecules Si(100)
[2 + 2] Cycloaddition
O–H dissociation

ABSTRACT

Competition between the C=C functional group with the OH group in allyl alcohol and with the C=O group in allyl aldehyde in the adsorption and thermal chemistry on Si(100)2×1 has been studied by X-ray photoelectron spectroscopy (XPS) and temperature-programmed desorption (TPD), as well as density-functional theory (DFT) calculations. The similarities found in the C 1s and O 1s spectra for both molecules indicate that the O–H dissociation product for allyl alcohol and [2 + 2] C=O cycloaddition product for allyl aldehyde are preferred over the corresponding [2 + 2] C=C cycloaddition products. Temperature-dependent XPS and TPD studies further show that thermal evolution of these molecules gives rise to the formation of ethylene, acetylene, and propene on Si(100)2×1, with additional CO evolution only from allyl alcohol. The formation of these desorption products also supports that the [2 + 2] C=C cycloaddition reaction does not occur. In addition, the formation of SiC at 1090 K is observed for both allyl alcohol and allyl aldehyde. We propose plausible surface-mediated reaction pathways for the formation of these thermal evolution products. The present work illustrates the crucial role of the Si(100)2×1 surface in selective reactions of the Si dimers with the O–H group in allyl alcohol and with the C=O group in allyl aldehyde over the C=C functional group common to both molecules.

1. Introduction

Surface chemistry of multifunctional organic molecules on Si(100)2×1 has attracted a lot of attention in the past decade [1–7]. The electrophile–nucleophile character of the buckled silicon dimers [8,9] on the Si(100)2×1 surface provides unique control of how this surface reacts with different functional groups. The buckling of the Si dimers enables the [2 + 2] cycloaddition reaction with alkene at room temperature (RT), which is normally symmetry-forbidden in classical chemistry by the Woodward–Hoffman selection rules [10]. To date, surface reactions of alkenes (with the C=C functional group) [6,11–24], aldehydes [25,26] and ketones (both with the C=O functional group) [25,27,28] on Si(100)2×1 have been reported to form [2 + 2] and [4 + 2] cycloaddition products, while those of alcohols (with the OH functional group) [29–34], carboxylic acids (with the COOH functional group) [35–44], and primary and secondary amines have resulted in H dissociation products [1,5,6]. These studies illustrate the critical role of the silicon surface in mediating selective chemical reactions largely involving a single functional group.

In order to investigate the selectivity of the 2 × 1 surface toward the aforementioned functional groups, we employ a molecule that contains multiple functional groups as the adsorbate, and study its thermal surface chemistry by using X-ray photoelectron spectroscopy (XPS) and temperature-programmed desorption (TPD), along with density-functional theory (DFT) calculations. In our recent work on acrylic acid [44], the simplest unsaturated carboxylic acid containing two functional groups, we compared the reactivity of the carboxyl group and ethenyl group in this bifunctional molecule with those of saturated carboxylic acids: acetic acid [43] and propanoic acid, both containing just the carboxyl group [44]. In particular, we showed that the Si(100)2×1 surface selectively favours O–H dissociation of the carboxyl group over [2 + 2] C=C cycloaddition of the ethenyl group and other possible reaction products in acrylic acid. As was also found for acetic acid [43] and propanoic acid [44], O–H dissociation in acrylic acid also leads to bidentate and unidentate carboxylate adspecies.

Using the ethenyl group as the "reference" functional group, we now extend our study of relative reactivity and selectivity of the carboxyl group [44] to other functional groups in a bifunctional molecule on Si(100)2×1. In particular, allyl alcohol (or 2-propenol, CH_2=CH–CH_2OH) and allyl aldehyde (or 2-propenal, CH_2=CH–CHO) offer the hydroxyl group (OH) and carbonyl group (C=O), respectively, as the second functional group, in addition to the

* Corresponding author.
E-mail address: tong@uwaterloo.ca (K.T. Leung).

0039-6028/$ - see front matter © 2009 Elsevier B.V. All rights reserved.
doi:10.1016/j.susc.2009.03.005

common ethenyl group (CH_2=CH−). In acrylic acid [44] (and carboxylic acids in general), the carboxyl group itself could be considered as consisting of two smaller functional groups, the OH and C=O. The present work, in effect, compares the competition of the ethenyl group with each of these smaller functional groups individually in their reactions with the 2×1 surface. To date, no experimental study has been reported for the adsorption of allyl alcohol and allyl aldehyde on Si(100)2×1. Only one DFT computational study [using the B3LYP/6−31G(d) method] of allyl alcohol on model Si(100) and Ge(100) cluster surfaces has been reported by Li et al. [45]. Their calculations showed that O–H dissociation results in more thermodynamically favourable products than [2 + 2] C=C cycloaddition products.

In the present work, we present XPS and TPD studies to follow the thermal evolution of the adsorption products of allyl alcohol and allyl aldehyde on Si(100)2×1. Together with our DFT calculations, these experimental results show that for allyl alcohol O−H dissociation is preferred over [2 + 2] C=C cycloaddition, as was proposed by Li et al. [45] and was also observed for other carboxylic acids [41,44]. For allyl aldehyde, [2 + 2] C=O cycloaddition is found to be more favourable than [2 + 2] C=C cycloaddition by our XPS measurement, in spite of the less negative calculated adsorption energy obtained for the former product than that for the latter by our DFT calculation. The present work therefore further affirms the remarkable stability of the ethenyl group relative to any of the following functional groups: OH, C=O (this work), COOH [44], and Cl [46,47] as well as other heteroatom-containing groups [6], on the 2×1 surface. These latter functional groups (except Cl) can therefore be used as the linkage to connect the molecule to the 2×1 surface, leaving the ethenyl group free for further reactions. Furthermore, the present experimental result also shows that multiple linkages through simultaneous interactions of two functional groups with the surface (such as the [O, C, C] tridentate and the [O, C] bidentate adstructures) do not occur, despite the considerably more negative adsorption energy calculated for these multiply bonded adstructures. The formation of ethylene, acetylene, and propene fragments found in our TPD experiments for both allyl alcohol and allyl aldehyde adspecies further supports that the common unreacted moiety (the ethenyl group) remains intact and free to undergo further thermal chemistry upon adsorption on Si(100)2×1.

2. Experimental and computational details

All of the experiments were performed in a home-built, dual-chamber ultrahigh vacuum system with a base pressure better than 1×10^{-10} Torr. Our experimental setup and procedure have been described in detail elsewhere [48]. Briefly, the sample preparation chamber was equipped with an ion sputtering gun, and a four-grid retarding-field optics for both reverse-view low energy electron diffraction and Auger electron spectroscopy. A 14×10 mm^2 substrate was cut from a single-side polished, p-type B-doped Si(100) wafer (0.4 mm thick) with a resistivity of 0.0080–0.0095 Ω cm. The Si substrate was pre-cleaned in the preparation chamber by cycles of Ar^+ sputtering (20 mA emission current, 1.5 kV beam energy) for 20 min at RT followed by annealing to 900 K for 5 min. The substrate was then flash-annealed to 1100 K for 20 s to obtain the 2×1 reconstructed surface. The cleanliness of the 2×1 surface was verified by the sharpness of the electron diffraction pattern and by our XPS data that showed no significant contamination. The clean Si substrate was then exposed to allyl alcohol (99.0% purity) or allyl aldehyde (90.0% purity), both purchased from Sigma–Aldrich, after appropriate thorough degassing of the colorless liquid chemicals by repeated freeze-pump-thaw cycles. All exposures were performed at RT by using a variable leak valve with the pressure monitored by an uncorrected ionization gauge, and reported in units of Langmuir (1 L = 10^{-6} Torr s). The high purity of the exposed chemical was confirmed by its cracking pattern obtained in situ. Saturation exposures were used for both the TPD and temperature-dependent XPS experiments unless stated otherwise.

TPD mass spectrometry and XPS experiments were conducted in the analysis chamber. For the TPD studies, a differentially pumped 1–300 amu quadrupole mass spectrometer (VG Quadrupole SXP Elite) was used, along with a home-built programmable proportional–integral–differential temperature controller to provide linear temperature ramping at an adjustable heating rate, typically set at 2.0 K s^{-1}. A type-K thermocouple (wrapped in a Ta foil) was mechanically placed in good contact with the front face of the sample to measure the temperature. The temperature of desorption maximum for the recombinative desorption of H_2 was used to calibrate the temperature scale [49]. To ensure that the selected mass fragments originate only from the species desorbed from the Si surface, the sample was positioned within 1 mm to the orifice (2 mm dia.) at the entrance of the differentially pumped housing of the mass spectrometer. Unless stated otherwise, the desorption profiles have been smoothed by adjacent averaging for clarity. For the XPS experiments, an electron spectrometer (VG Scientific CLAM-2), consisting of a hemispherical analyser of 100 mm mean radius and a triple-channeltron detector, was used, along with a twin-anode X-ray source that supplied unmonochromatic Al K_α radiation (1486.6 eV photon energy). XPS spectra were collected with an acceptance angle of ±4° at normal emission from the silicon sample, and with a constant pass energy of 50 eV, giving an effective energy resolution of 1.4 eV full-width-at-half-maximum for the Si 2p photopeak. The binding energy scale of the XPS spectra has been calibrated to the Si 2p feature of the bulk at 99.3 eV. Spectral peak fitting based on residual minimization with Gaussian–Lorentzian lineshapes was performed by using the CasaXPS software. For temperature-dependent XPS measurements, the sample was flash-annealed to the preselected temperature and cooled back to RT before collecting the XPS spectra.

The DFT [50] method in the Gaussian 03 software package [51] was used to calculate the electronic structures of the adstructures. The hybrid B3LYP functional, composed of Becke's three-parameter gradient-corrected exchange functional [52] and the Lee–Yang–Parr correlation functional [53], was employed. The DFT/B3LYP method has been shown to provide generally good agreement with the experimental data for the adsorption of many molecular systems on Si(100)2×1 [5]. We performed the present calculations using four basis sets: 6−31G(d), 6−31+G(d), 6−31++G(d) and 6−31++G(d,p), all of which gave similar results for the optimized geometries and total energies (with the larger basis set providing a lower total energy). Frequency calculations were also performed for all of the optimized geometries, in order to ascertain that the local minima correspond to the equilibrium structures and not transition-state structures. In the present work, the Si(100)2×1 surface was simulated by the double-dimer surface of a $Si_{15}H_{16}$ cluster. The adstructures of allyl alcohol and allyl aldehyde were fully optimized without any geometrical constraint on the $Si_{15}H_{16}$ cluster. The corresponding adsorption energy (for allyl alcohol and allyl aldehyde), ΔE, was estimated by the difference between the total energy for an optimized structure of the adsorbate–substrate configurations (ASCs) of the adsorbate on the $Si_{15}H_{16}$ model surface and the sum of the total energies of the free molecule and of the $Si_{15}H_{16}$ cluster. All the total energies were obtained without zero-point correction and no basis set superposition error correction was made to ΔE.

3. Results and discussion

3.1. DFT computational study of adsorbate–substrate configurations

Fig. 1 shows four plausible adstructures on the double-dimer model surface of the $Si_{15}H_{16}$ cluster, involving O–H dissociation (ASC I) and [2 + 2] C=C cycloaddition (ASC II) for allyl alcohol, and [2 + 2] C=O cycloaddition (ASC IV) and [2 + 2] C=C cycloaddition (ASC V) for allyl aldehyde. Table 1 summarizes the calculated adsorption energies and total energies of the four ASCs obtained with four different basis sets: 6–31G(d), 6–31+G(d), 6–31++G(d), and 6–31++G(d,p). Evidently, all four basis sets provide very similar values, with the larger basis set generally giving a lower total energy but a less negative adsorption energy. There is a more notable change in the adsorption energy between the 6–31G(d) and the next larger basis set [6–31+G(d)] than that between the larger basis sets. The change between the 6–31++G(d) and the largest 6–31++G(d,p) basis sets appears to be more noticeable for ASC I, likely due to the improved modeling of the diffuse bonding involving O–H dissociation. The results obtained with the largest 6–31++G(d,p) basis set will be used for the following discussion.

Evidently for allyl alcohol, the adsorption energy (and total energy) for the O–H dissociation product (−249.4 kJ mol^{-1}, Fig. 1a) is considerably more negative than that for the [2 + 2] C=C cycloaddition product (−169.1 kJ mol^{-1}, Fig. 1b). The dative bonding between O and the electron-deficient site of the Si dimer leads to the attachment of allyl alcohol to Si through O followed by O–H dissociation to eventually form ASC I. For the less stable ASC II, the reduction of the π bond results in the formation of two Si–C bonds in the cycloaddition reaction, which is expected to give a lower C 1s binding energy (BE) than that in C–C and C=C. For allyl aldehyde, the calculated adsorption energy of the [2 + 2] C=O cycloaddition product (−164.7 kJ mol^{-1}, Fig. 1d) is found to be less negative than that of [2 + 2] C=C cycloaddition product (−174.8 kJ mol^{-1}, Fig. 1e). However, the similarity of these values indicates that both ASCs IV and V are equally probable thermodynamically. The presence of C=C only in ASC IV should give rise to notable difference in the C 1s BE between ASCs IV and V, which would allow us to distinguish these structures from our XPS measurement (to be discussed below).

Our frequency calculations show that the wavenumbers for C–O (1071 cm^{-1}) and C=C stretching vibrations (1715 cm^{-1}) for

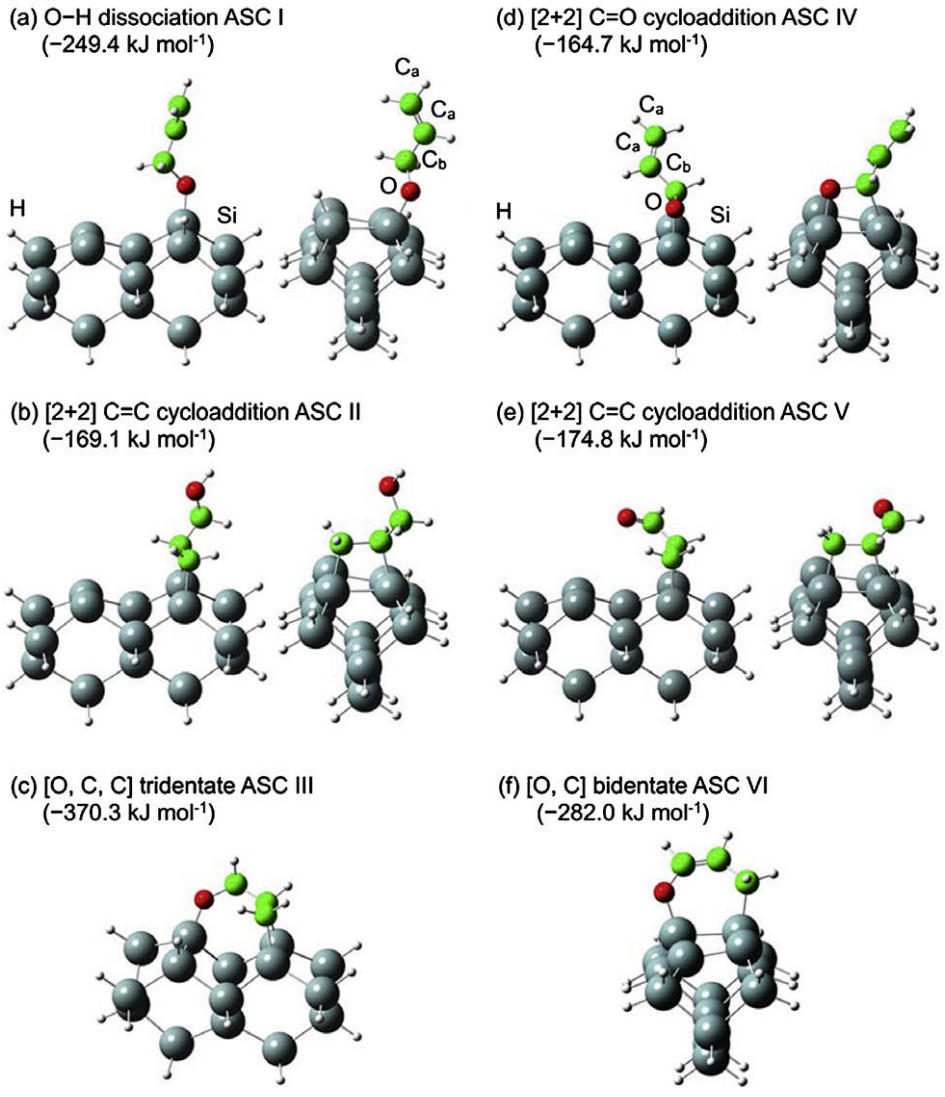

Fig. 1. Optimized geometries of the adsorbate–substrate configurations (ASCs): (a) O–H dissociation ASC I, (b) [2 + 2] C=C cycloaddition ASC II, and (c) [O, C, C] tridentate ASC III products of allyl alcohol, and (d) [2 + 2] C=O cycloaddition ASC IV, (e) [2 + 2] C=C cycloaddition ASC V and (f) [O, C] bidentate ASC VI products of allyl aldehyde, all on Si(100)2×1. The corresponding adsorption energies calculated with the 6–31++G(d,p) basis set are given in parentheses.

Table 1
Comparison of the adsorption energies, ΔE, and total energies (in square parentheses) for plausible adsorbate–substrate configurations (ASCs) of allyl alcohol and allyl aldehyde on Si(100)2×1 obtained by DFT/B3LYP calculations with 6−31G(d), 6−31+G(d), 6−31++G(d), and 6−31++G(d,p) basis sets.

ΔE (kJ mol^{-1}) [total energy (hartree)]	6−31G(d)	6−31+G(d)	6−31++G(d)	6−31++G(d,p)
O–H dissociation ASC I	−276.7 [−4545.27532]	−261.0 [−4545.29652]	−261.1 [−4545.29823]	−249.4 [−4545.32457]
[2 + 2] C=C cycloaddition ASC II	−175.6 [−4545.23682]	−169.3 [−4545.26162]	−169.7 [−4545.26340]	−169.1 [−4545.29397]
[2 + 2] C=O cycloaddition ASC IV	−173.1 [−4545.03698]	−163.8 [−4545.05824]	−163.9 [−4545.05981]	−164.7 [−4545.08393]
[2 + 2] C=C cycloaddition ASC V	−185.2 [−4545.04158]	−174.9 [−4545.06246]	−174.9 [−4545.06401]	−174.8 [−4545.08776]

ASC I are slightly higher than the corresponding calculated values for isolated allyl alcohol molecule (1045 cm^{-1} and 1708 cm^{-1}, respectively). Similarly, the wavenumber for C=C stretch (1692 cm^{-1}) for ASC IV is also essentially the same as the corresponding calculated value for isolated allyl aldehyde molecule (1683 cm^{-1}). The similarity in the wavenumbers for C=C vibrations in ASC I and ASC IV to those of their respective isolated allyl alcohol and allyl aldehyde molecules is not surprising, because the ethenyl group is not directly involved in binding to the surface. On the other hand, no corresponding calculated wavenumber for C=C is found for ASC II and ASC V due to the formation of C–C bonding as a result of [2 + 2] cycloaddition.

Our DFT calculation also reveals two unique, multiply bonded ASCs, including an [O, C, C] tridentate CH_2–CH–CH_2–O complex obtained from [2 + 2] C=C cycloaddition and O–H dissociation of allyl alcohol (Fig. 1c), and an [O, C] bidentate CH_2–CH=CH–O complex derived from the delocalized form (CH_2···CH···CH···O) of allyl aldehyde (Fig. 1f). Despite having the most negative adsorption energies, these ASCs are improbable due to kinetic effects and the need for additional molecular motions to facilitate the required multiple attachments to the Si(100)2×1 surface. As discussed below, these ASCs can be ruled out by our XPS measurement.

3.2. Room-temperature adsorption of allyl alcohol and allyl aldehyde on Si(100)2×1

In the present work, we have carried out XPS measurements for a number of exposures of allyl alcohol and of allyl aldehyde on Si(100)2×1, ranging from 0.1 L to 120 L. The saturation exposure for allyl aldehyde (60 L) is found to be discernibly lower than that for allyl alcohol (106 L), in good agreement with the generally higher reactivity of aldehyde relative to alcohol.

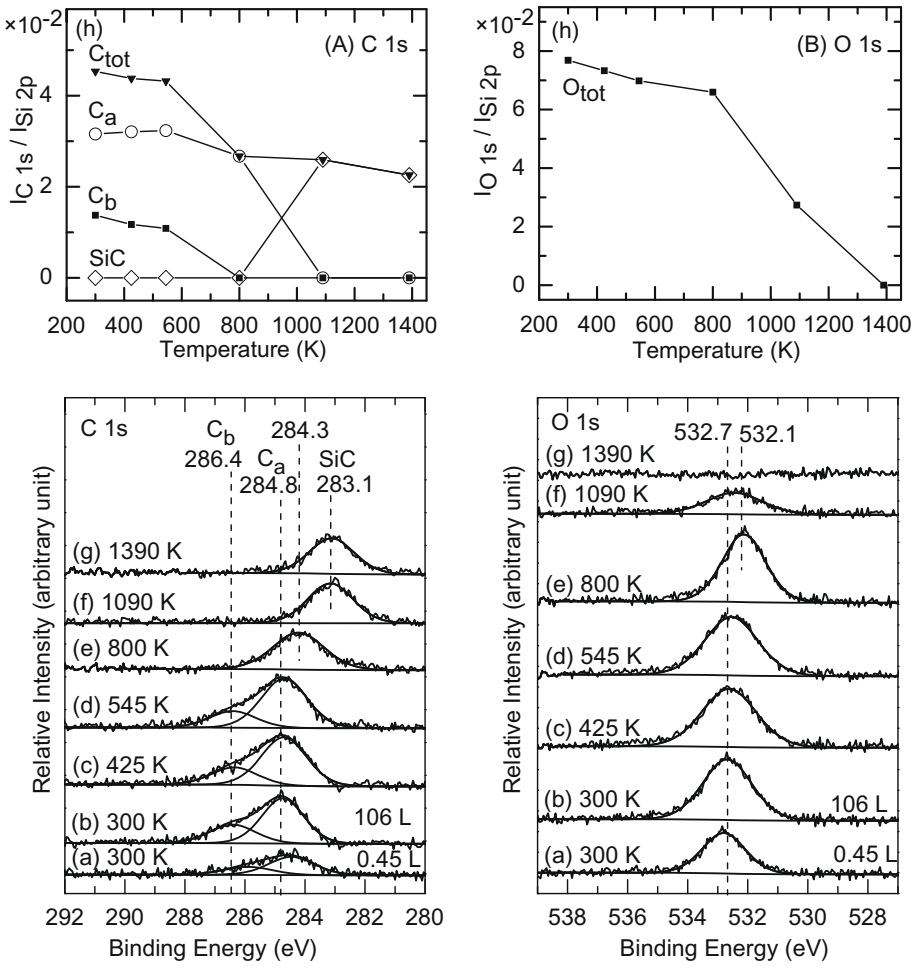

Fig. 2. XPS spectra of the C 1s (left column) and O 1s regions (right column) for (a) a 0.45 L and (b) a saturated exposures (106 L) of allyl alcohol deposited on Si(100)2×1 at 300 K, and for sample (b) upon sequential flash-annealing to (c) 425 K, (d) 545 K, (e) 800 K, (f) 1090 K, and (g) 1390 K. (h) Corresponding temperature profiles of the C 1s intensities ($I_{C\ 1s}$) for SiC at 283.1 eV, C_a at 284.3–284.8 eV, and C_b at 286.4 eV, along with the total intensity for C 1s (C_{tot}), and of the total O 1s intensity ($I_{O\ 1s}$), all with respect to the intensity of Si 2p ($I_{Si\ 2p}$).

Fig. 2 shows the XPS spectra of the C 1s and O 1s regions for a low exposure (0.45 L) and a saturation exposure (106 L) of allyl alcohol deposited on Si(100)2×1 at RT. The C 1s spectra for both exposures exhibit a single broad band, which we appropriately fitted with two Gaussian profiles, each with an approximate width of 1.8 eV full-width-at-half-maximum (FWHM), in order to identify the prominent C local chemical environments. In marked contrast to the XPS results for acetic acid [43], acrylic acid and propanoic acid [44], similar features are obtained at both low and high RT exposures for allyl alcohol on Si(100)2×1, suggesting the presence of adstructures with similar C 1s environments for both low and high exposures. In particular, the C 1s features at BEs of 284.8 eV and 286.4 eV are found to have, respectively, relative integrated intensities of 0.031 and 0.014 (with an approximate intensity ratio of 2:1) with respect to the intensity of Si 2p for both low (Fig. 2Aa) and saturation exposures (Fig. 2Ab). The C 1s BEs for the C=O, C–O, C=C, C–C, C–Si bonds are generally found at 287.8–288.5 eV [25–27], 285.4–286.9 eV [25–27,34], 284.8–285 eV [14,17,20], 284.4 eV [17,20] and 283.7–284.3 [14,17,20,27], respectively. The absence of the C–Si feature below 284.3 eV in our C 1s spectra could therefore be used to rule out the existence of ASC II (Fig. 1b) and ASC III (Fig. 1c). The observation of the C 1s features at 284.8 eV (C_a) and 286.4 eV (C_b) attributed to C=C and C–O moieties, respectively, indicates the predominant formation of ASC I. Given the higher electronegativity of O (3.5, Pauling scale) with respect to C (2.5) [10], C_b (with an O atom attached) should be partially positively charged and it should therefore exhibit a higher C 1s BE than the ethenyl (CH_2=CH–) carbons (C_a), as observed in Fig. 2Aa. The nearly constant C 1s intensity ratio of C_a:C_b with respect to exposure (Fig. 2Aa and Ab) suggests that no new ASC (other than ASC I) is formed at a higher exposure. The C_a:C_b value of 2:1 is also in excellent accord with the stoichiometric ratio of C_a to C_b in ASC I. In the case of O 1s, the corresponding BE observed at 532.7 eV (Fig. 2Ba and Bb) is not very useful for identifying the adstructures (i.e. between ASC I and ASC II/III) because of the similarity in the electronegativities of Si (1.8) and H (2.1) and the generally broad widths found for the O 1s peaks.

The XPS spectra of the C 1s and O 1s regions for a low exposure (0.2 L) and a saturation exposures (60 L) of allyl aldehyde on Si(100)2×1 at RT, shown in Fig. 3, are found to be remarkably similar to those of allyl alcohol (Fig. 2). In particular, two Gaussian profiles at 284.7 eV and 286.3 eV, each with a width of 1.6 eV FWHM, can be fitted to the broad C 1s bands observed for both exposures, giving relative integrated intensities of 0.037 and 0.019 with an approximate intensity ratio of 2:1. As with the allyl alcohol case (Fig. 2), the BE positions of the observed C 1s peaks at 284.7 eV (C_a) and 286.3 eV (C_b) (Fig. 3) correspond to the C=C and C–O bonds, consistent with the [2 + 2] C=O cycloaddition product

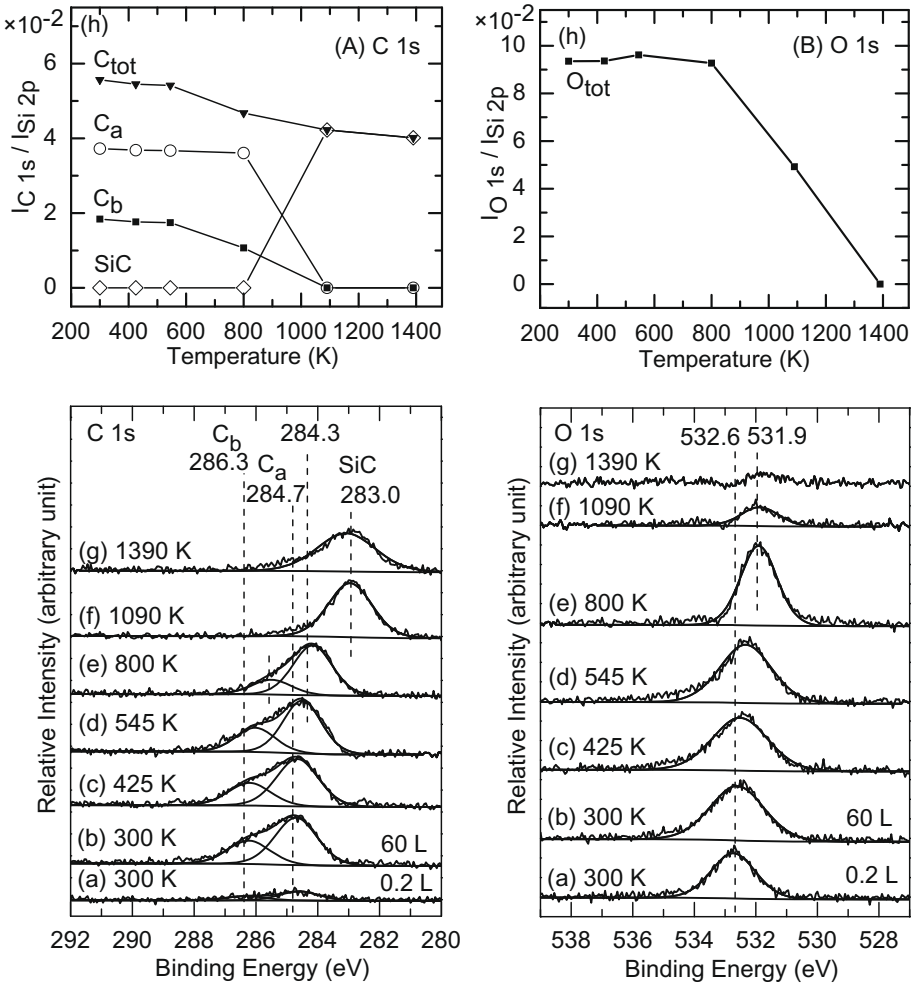

Fig. 3. XPS spectra of the C 1s (left column) and O 1s regions (right column) for (a) a 0.2 L and (b) a saturated exposures (60 L) of allyl aldehyde deposited on Si(100)2×1 at 300 K, and for sample (b) upon sequential flash-annealing to (c) 425 K, (d) 545 K, (e) 800 K, (f) 1090 K, and (g) 1390 K. (h) Corresponding temperature profiles of the C 1s intensities ($I_{C\ 1s}$) for SiC at 283.0 eV, C_a at 284.3–284.7 eV, and C_b at 286.3 eV, along with the total intensity for C 1s (C_{tot}), and of the total O 1s intensity ($I_{O\ 1s}$), all with respect to the intensity of Si 2p ($I_{Si\ 2p}$).

(ASC IV). It should be noted that, despite the difference in the local chemical environment of C_b between ASC IV (bonded to Si) and ASC I (bonded to H), the corresponding BEs are found to be essentially the same because of the similar electronegativities for Si (1.8) and H (2.1). The observed C 1s BE positions for C_a and C_b also rule out the formation of [2 + 2] C=C cycloaddition product (ASC V), because no signatures of C–Si (expected at 283.7–284.3 eV) [14,17,20,27] and C=O (at 287.8–288.5 eV) [25–27] are observed in the C 1s spectra (Fig. 3). Despite the discernibly more negative adsorption energy for ASC V (Fig. 1e) than that for ASC IV (Fig. 1d) obtained in the DFT calculations, the present XPS measurement is therefore instrumental in identifying the adsorption structures. In contrast to the C=C bond, the asymmetric electron density of the C=O bond is more compatible with the electrophile–nucleophile character of the Si=Si dimer, which favours the formation of [2 + 2] C=O cycloaddition product. Furthermore, we can also rule out the formation of [O, C] bidentate ASC VI (Fig. 1f), because three distinct C 1s features corresponding to C–Si, C=C, and C–O (with equal intensity) expected for this structure are not observed. In addition, the O 1s feature at 532.6 eV shown in Fig. 3Ba and Bb for allyl aldehyde is also found at the similar position to that of allyl alcohol (532.7 eV, Fig. 2Ba and Bb). This similarity is not surprising because the O atom is attached to a Si and a C_b atoms in both ASC I (Fig. 1a) and ASC IV (Fig. 1d).

3.3. Thermal evolution of allyl alcohol and allyl aldehyde adspecies on Si(100)2×1

Figs. 2 and 3 also show the C 1s and O 1s XPS spectra for RT saturation exposures of allyl alcohol and allyl aldehyde, respectively, on Si(100)2×1 upon successive flash-annealing to selected temperatures. Evidently, the C_b 1s peak for O–H dissociation product (ASC I) of allyl alcohol (Fig. 1a) at 286.4 eV decreases in intensity gradually upon annealing to 545 K (Fig. 2Ad) and disappears completely after annealing to 800 K (Fig. 2Ae). For the ethenyl C_a 1s peak at 284.8 eV, little change to the intensity is observed up to the annealing temperature of 545 K. Upon further annealing to 800 K, the C_a 1s peak position appears to shift to a lower BE (284.3 eV) and undergoes a small reduction in intensity due to possible fragmentation and desorption of the smaller fragments. Continued annealing to 1090 K completely removes the C_a 1s feature (Fig. 2Af), and introduces a new feature at 283.1 eV, commonly attributed to SiC, the intensity of which remains unchanged at the highest annealing temperature of 1390 K (Fig. 2Ag). The latter could be due to dehydrogenation of the remaining C_a containing fragments and its conversion to SiC on the surface in this temperature range. In Fig. 2Ah, we summarize the observed intensity changes of these three C 1s features (C_a, C_b, and SiC) along with the total C 1s intensity, all relative to the intensity of Si 2p, as a function of the annealing temperature. The temperature profiles clearly indicate the presence of a transition region between 545 K and 1090 K, where thermal desorption and fragmentation occur. It is of interest to note that nearly 45% of the total C (corresponding to almost all of the C_b and some of the C_a) has been eliminated from the surface upon annealing to 800 K, with the remaining converted to SiC that cannot be removed even at the annealing temperature of 1390 K. The corresponding temperature profile for the O 1s feature, shown in Fig. 2Bh, depicts a gradual reduction in intensity up to 800 K, followed by a marked decrease upon further annealing to 1390 K. Between the annealing temperature of 545 K and 800 K, the O 1s feature has evidently become sharper and shifted from 532.7 eV (Fig. 2Bd) to a slightly lower BE of 532.1 eV (Fig. 2Be). This spectral change suggests that part of the O-containing moiety has undergone dissociation and/or desorption from the surface, producing Si–O on the surface with a lower O 1s BE. The reduction in the O 1s intensity above 800 K is likely due to desorption of SiO fragments or O diffusion into the bulk.

For a saturation exposure of allyl aldehyde on Si(100)2×1, the corresponding spectral changes in the C 1s and O 1s features as a function of annealing temperature (Fig. 3) appear to be similar to those found for allyl alcohol (Fig. 2). In particular, the C_a 1s temperature profile for allyl aldehyde (Fig. 3Ah) closely follows that of for allyl alcohol (Fig. 2Ah), with minimal reduction in intensity upon annealing to 800 K followed by complete extinction after further annealing to 1090 K. A notable difference observed in the C_b 1s temperature profile for allyl aldehyde (Fig. 3Ah) from that for allyl alcohol (Fig. 2Ah) is that the temperature of its complete extinction occurs at a higher annealing temperature (1090 K) for the former than that for the latter (800 K). The C 1s spectrum for the 800 K annealing temperature (Fig. 3Ae) appears to have shifted to the lower BE side. The small shift to the lower BE found for C_a 1s (284.3 eV) is consistent with the attachment of an ethenyl group (with the C 1s peak commonly found at 283.9 eV) [46], after dissociation from the $\underline{C}H–\underline{O}$ moiety attached to the Si surface (Fig. 1d) at 800 K. The dissociation removes the effectively electron withdrawing ethenyl group and reduces the partial positive charge on the C of the remaining di-σ bonded $\underline{C}H–\underline{O}$ moiety, causing the C_b 1s peak to shift to a lower BE (285.5 eV). For allyl aldehyde, the related peak for SiC at 283.0 eV (Fig. 3Ae) is found at a similar annealing temperature (1090 K) (Fig. 3Af) as that for allyl alcohol (Fig. 2Af). In accord with the allyl alcohol case, SiC begins to form above 800 K (Fig. 3Af) and the spectral intensity becomes slightly reduced upon further annealing from 1090 K to 1390 K. Furthermore, nearly 80% of the total C of the adsorbed allyl aldehyde has been converted to SiC, in marked contrast to allyl alcohol where only 55% of the C remains as SiC. This difference in the SiC formation indicates more C-containing desorbates for allyl alcohol than allyl aldehyde, which suggests limited desorption channels for the C-containing species for allyl aldehyde on Si(100)2×1. For the O 1s temperature profile, there is virtually no change in the O 1s intensity for allyl aldehyde up to 800 K (Fig. 3Bh), in contrast to the early onset of the gradual reduction in O 1s intensity at 425 K for allyl alcohol (Fig. 2Bh). This difference in the onset temperature suggests that more energy is required for the dissociation or formation of O-containing fragments for allyl aldehyde than allyl alcohol. Above 800 K, the O 1s intensities for both allyl aldehyde and allyl alcohol evidently undergo marked reduction, with total removal at 1390 K.

In addition to the temperature profiles obtained from our XPS measurements that depict the thermal evolution of the adspecies remaining on the 2 × 1 surface, we also performed TPD experiments to follow the desorption products that evolve from the surface as a function of temperature. Fig. 4 compares the TPD profiles of selected mass fragments with m/z 2, 26, 27, 28, 39, 40, 41, and 42 for a RT saturation exposure of allyl alcohol and of allyl aldehyde on Si(100)2×1. We also monitored other mass fragments, including m/z 30 ($CH{=}OH^+$), and m/z 31 ($CH_2{=}OH^+$), and m/z 57 ($CH_2{=}CH–CH{=}OH^+$ or the parent mass) of allyl alcohol, as well as m/z 55 ($CH_2{=}CH–C{\equiv}O^+$) and m/z 56 ($CH_2{=}CH–CHO^+$ or the parent mass) of allyl aldehyde [54]. Except for the observed TPD profiles of the masses shown in Fig. 4, none of the other monitored masses exhibits any TPD features, which suggests that neither allyl alcohol nor allyl aldehyde adsorbs molecularly on Si(100)2×1 at RT. For both allyl alcohol and allyl aldehyde, the most intense desorption feature is observed for m/z 2 at 810 K (Fig. 4Aa and Ba), which corresponds to recombinative desorption of H_2 from silicon monohydrides [49].

For allyl alcohol on Si(100)2×1, the TPD profile for m/z 26 exhibits two peaks at 585 K and 770 K (Fig. 4Ab). Given that the cracking pattern of propene ($CH_2{=}CH–CH_3$) contains m/z 26 ($C_2H_2^+$), m/z 27 ($C_2H_3^+$), m/z 39 ($C_3H_3^+$), m/z 40 ($C_3H_4^+$), m/z 41

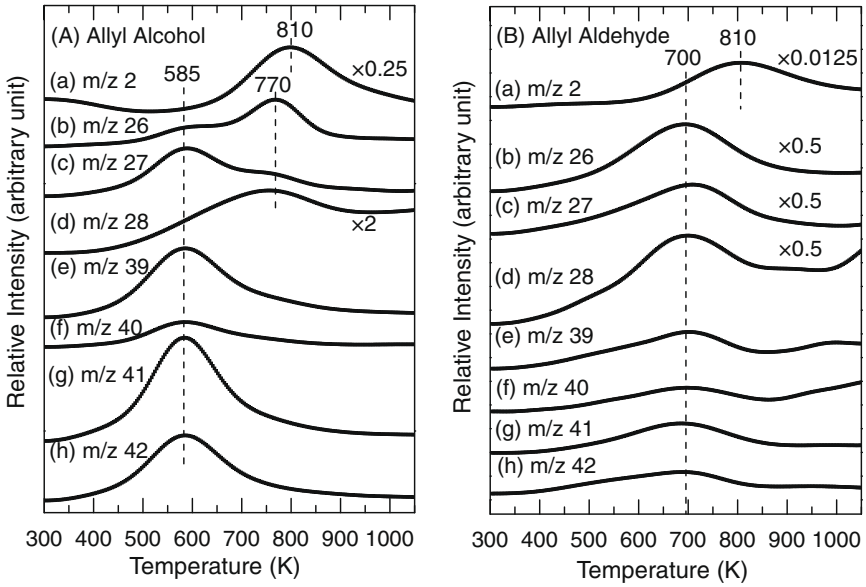

Fig. 4. TPD profiles of selected fragments of m/z (a) 2, (b) 26, (c) 27, (d) 28, (e) 39, (f) 40, (g) 41, and (h) 42 for a saturation exposure of (A) allyl alcohol and (B) allyl aldehyde on Si(100)2×1 deposited at 300 K.

($C_3H_5^+$, base mass) and m/z 42 ($C_3H_6^+$, parent mass) [54], the weak m/z 26 peak found at the same temperature as those of these other mass fragments (585 K, Fig. 4A) therefore supports the molecular desorption of propene. The stronger m/z 26 peak at 770 K corresponds to desorption of acetylene (with m/z 26 as its parent and base masses), in accord with similar desorption temperature found in earlier work [46,47]. Furthermore, the TPD profiles of m/z 28 ($C_2H_4^+$, parent and base masses) and m/z 27 ($C_2H_3^+$), corresponding to the cracking pattern of ethylene, also reveal a peak maximum at 770 K, suggesting that the desorption of both acetylene and ethylene fragments comes from a common source. (It should be noted that the cracking pattern of ethylene also includes m/z 26, present as a minor component.) The broad TPD profile of m/z 28, with a significant desorption intensity over 450–850 K not accountable in the TPD profile of m/z 27, therefore suggests additional contribution from CO (with parent mass of m/z 28), in good accord with our temperature-dependent XPS data (Fig. 2Ah and Bh), which shows intensity reduction of both C_b 1s and O 1s upon annealing in this temperature range.

Similar to allyl alcohol, allyl aldehyde also exhibits TPD profiles with desorption maxima at 700 K for m/z 39, m/z 40, m/z 41, and m/z 42 (Fig. 4Be–h), but with considerably weaker intensities. These desorption features can be attributed to propene desorption, and the observed higher desorption temperature (700 K, compared to that found for allyl alcohol, 585 K) suggests that propene production requires a higher energy pathway for allyl aldehyde than that for allyl alcohol. The rather weak desorption intensity of the base mass, m/z 41, for propene desorption also indicates that the corresponding contributions to m/z 26 and m/z 27 from propene desorption cannot account for the strong desorption intensities found for these two masses, suggesting additional sources. The strong desorption features at 700 K found for m/z 26, m/z 27, and m/z 28 all correspond to the desorption of ethylene. However, given that the desorption maximum for m/z 26 (Fig. 4Bb) is almost the same as that of m/z 28 (the parent and base masses of ethylene), additional contribution likely from acetylene (with its parent and base masses at m/z 26) must be present. Unlike allyl alcohol (Fig. 2Bh), no loss of O 1s intensity over the 425–800 K annealing temperature range is observed for allyl aldehyde (Fig. 3Bh), which therefore suggests that the observed TPD profile for m/z 28 (Fig. 4Bd) does not have any contribution from CO desorption.

It is also of interest to note that the absolute desorption intensity (not shown) for any selected mass fragment observed for allyl aldehyde is found to be considerably smaller than that for allyl alcohol (by at least a factor of 20). This observation indicates that the adspecies of allyl aldehyde prefer dissociation over desorption, in good agreement with the corresponding higher total C 1s XPS signal after annealing to 1390 K found for allyl aldehyde (Fig. 3Ah) than that for allyl alcohol (Fig. 2Ah).

Fig. 5 shows the schematic pathways proposed for the formation of ethylene, acetylene, and propene as well as CO from the O–H dissociation product ASC I (Structure I) for allyl alcohol, and for the formation of ethylene, acetylene, and propene from the [2 + 2] C=O cycloaddition product ASC III (Structure II) for allyl aldehyde. It should be noted that the actual mechanisms likely follow more complicated reaction steps than that presented here, to only show the necessary bond dissociation involved in the formation of these desorbates. In particular, we present a similar model for the formation of ethylene and acetylene from the respective allyl alcohol and allyl aldehyde adstructures on the 2 × 1 surface. For both Structure I (Fig. 5A) and Structure II (Fig. 5B), a C–C bond cleavage produces a dissociated ethenyl radical (CH_2=$CH^{\cdot}$) that stays on the surface, generating the respective intermediates. The Ibc intermediate (Fig. 5A) subsequently abstracts a H atom likely from Si–H (Structure Ib) through pathway b or undergoes C–H dissociation in the cleaved surface ethenyl radical (Structure Ic) through pathway c, producing ethylene and acetylene, respectively. The remaining O–CH_2 fragment singly bonded to the surface could undergo total dissociation, producing the observed CO desorbate (and dissociated H atoms). Similarly, the IIfg intermediate (Fig. 5B) also abstracts a H atom from the surface (Structure IIf) through pathway f, producing ethylene, or undergoes C–H dissociation in the surface ethenyl radical (Structure IIg) through pathway g, producing acetylene. With the dissociated H_2C–O fragment firmly di-σ bonded to the Si surface, it is not surprising that CO cannot be released as a desorbate.

For the formation of propene desorbates from allyl alcohol (Fig. 5A), Structure I could undergo C–O dissociation (Structure Id) through pathway d to produce a propenyl radical (CH_2=CH–$CH_2^{\cdot}$), which becomes propene through abstraction of a H atom from the surface (Structure Id'). For allyl aldehyde, the formation of propene from Structure II (Fig. 5B) likely proceeds

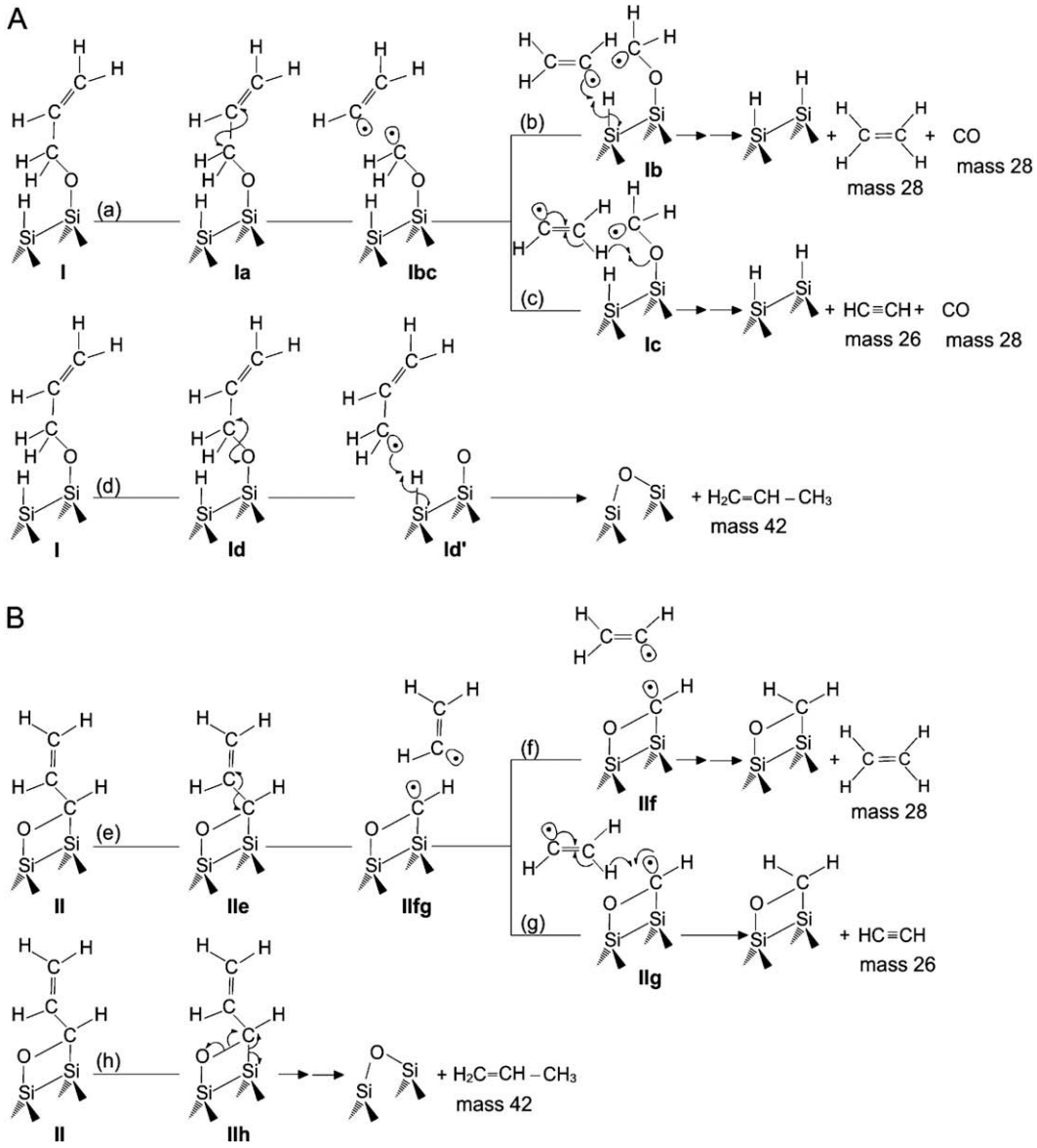

Fig. 5. Schematic models for thermal evolution of the O–H dissociation and [2 + 2] C=O cycloaddition products to ethylene, acetylene, and propene for (A) allyl alcohol and (B) allyl aldehyde, respectively, on Si(1 0 0)2×1, and to additional CO desorption for (A) allyl alcohol.

through pathway h involving C–O dissociation and double H abstraction, the mechanism of which is unclear. The generally higher temperature of the desorption maxima (700 K) observed for propene-related mass fragments (m/z 27, 39, 40, 41, and 42) from allyl aldehyde (Fig. 4B) relative to that (585 K) from allyl alcohol (Fig. 4A) is consistent with the higher energy required for the multi-step process expected from pathway h relative to that required for pathway d.

For m/z 26, 27, and 28, considerable desorption intensities are found over the 600–800 K range for both allyl alcohol and allyl aldehyde, in good accord with the similar bond dissociation energies required for the production of ethylene and acetylene. As depicted in Fig. 5, both Structures I and II involve C–C bond dissociation (with a typical bond dissociation energy of 385 kJ mol^{-1}) [55] to generate the ethenyl radical as the precursor, followed by Si–H (293 kJ mol^{-1}) and C–H dissociation (399 kJ mol^{-1}) to produce ethylene and acetylene, respectively. These pathways require rather similar energies, therefore giving rise to desorption intensities in the observed similar temperature range. In addition, for allyl alcohol on Si(1 0 0)2×1, the desorption maxima for propene desorption (585 K) have been found to be lower than those for ethylene and acetylene (770 K) (Fig. 4A). This observation is consistent with the preferred formation of the more stable propenyl radical in pathway d over the ethenyl radical in pathway a (Fig. 5A), which also accounts for the stronger desorption intensities found for the propene-related fragments than those for ethylene and acetylene.

4. Summary

XPS and TPD experiments have been performed for the first time on allyl alcohol and allyl aldehyde on Si(1 0 0)2×1. The C 1s and O 1s spectra of allyl alcohol show that the O–H dissociation product is preferred over the [2 + 2] C=C cycloaddition product, in agreement with the DFT calculation. For allyl aldehyde, even though DFT calculation shows that the adsorption energy for the [2 + 2] C=C cycloaddition product is more negative than the C=O cycloaddition product, our XPS data supports the formation of

the C=O cycloaddition product. These results are consistent with the efficacy of the electrophile O in allyl alcohol and of the electrophile–nucleophile C=O bond in allyl aldehyde in establishing direct interactions with the Si buckled dimer on the 2×1 surface. Furthermore, the combined temperature-dependent XPS and TPD data can be used to infer plausible thermal evolution pathways that lead to the observed formation of ethylene, acetylene, and propene, resulting from the O–H dissociation product of allyl alcohol and the [2 + 2] C=O cycloaddition product of allyl aldehyde. The formation of these desorption products reflects the selectivity of the directional dangling bonds on the Si(100)2×1 surface for preferred reactions with the hydroxyl and carbonyl groups over the ethenyl group. Desorption of CO is also observed from the former and not the latter, while the formation of SiC from the dissociated ethenyl group above 1050 K indicates the remarkable stability of the C=C bond. As bifunctional molecules that leave the ethenyl group intact upon adsorption on the 2×1 surface, allyl alcohol and allyl aldehyde, like acrylic acid, therefore serve as viable linker molecules to provide further functionalization of this important semiconductor surface.

Acknowledgements

This work was supported by the Natural Sciences and Engineering Research Council of Canada. Part of the calculations presented in the present work was performed at the WHALE cluster of the Shared Hierarchical Academic Research Computing Network supported by the governments of Canada and the province of Ontario. We are indebted to Professor Michael Chong for helpful discussions of various aspects of relevant organic chemistry.

References

[1] M.A. Filler, S.F. Bent, Prog. Surf. Sci. 73 (2003) 1.
[2] S.F. Bent, Surf. Sci. 500 (2002) 879.
[3] J.M. Buriak, Chem. Commun. (1999) 1051.
[4] J.M. Buriak, Chem. Rev. 102 (2002) 1271.
[5] X. Lu, M.C. Lin, Int. Rev. Phys. Chem. 21 (2002) 137.
[6] T.R. Leftwich, A.V. Teplyakov, Surf. Sci. Rep. 63 (2008) 1.
[7] R.A. Wolkow, Annu. Rev. Phys. Chem. 50 (1999) 413.
[8] R.A. Wolkow, Phys. Rev. Lett. 68 (1992) 2636.
[9] H.N. Waltenburg, J.T. Yates Jr., Chem. Rev. 95 (1995) 1589.
[10] F.A. Carey, Organic Chemistry, 3rd ed., McGraw-Hill, Toronto, 1996.
[11] C.C. Cheng, R.M. Wallace, P.A. Taylor, W.J. Choyke, J.T. Yates Jr., J. Appl. Phys. 67 (1990) 3693.
[12] L. Clemen, R.M. Wallace, P.A. Taylor, M.J. Dresser, W.J. Choyke, W.H. Weinberg, J.T. Yates Jr., Surf. Sci. 268 (1992) 205.
[13] A.J. Mayne, A.R. Avery, J. Knall, T.S. Jones, G.A.D. Briggs, W.H. Weinberg, Surf. Sci. 284 (1993) 247.
[14] M. Ikeda, T. Maruoka, N. Nagashima, Surf. Sci. 416 (1998) 240.
[15] J.S. Hovis, H.B. Li, R.J. Hamers, J. Phys. Chem. B 102 (1998) 6873.
[16] M.J. Kong, A.V. Teplyakov, J. Jagmohan, J.G. Lyubovitsky, C. Mui, S.F. Bent, J. Phys. Chem. B 104 (2000) 3000.
[17] H. Liu, R.J. Hamers, Surf. Sci. 416 (1998) 354.
[18] M. Kiskinova, J.T. Yates Jr., Surf. Sci. 325 (1995) 1.
[19] H.B. Liu, R.J. Hamers, J. Am. Chem. Soc. 119 (1997) 7593.
[20] J.S. Hovis, R.J. Hamers, J. Phys. Chem. B 101 (1997) 9581.
[21] L.C. Teague, J.J. Boland, J. Phys. Chem. B 107 (2003) 3820.
[22] H.S. Kato, M. Wakatsuchi, M. Kawai, J. Yoshinobu, J. Phys. Chem. C 111 (2007) 2557.
[23] R.J. Hamers, Y. Wang, Chem. Rev. 96 (1996) 1261.
[24] R.J. Hamers, S.K. Coulter, M.D. Ellison, J.S. Hovis, D.F. Padowitz, M.P. Schwartz, C.M. Greenlief, J.N. Russell Jr., Acc. Chem. Res. 33 (2000) 617.
[25] J.L. Armstrong, J.M. White, M. Langell, J. Vac. Sci. Technol. A 15 (1997) 1146.
[26] H.G. Huang, Y.P. Zhang, Y.H. Cai, J.Y. Huang, K.S. Yong, G.Q. Xu, J. Chem. Phys. 123 (2005) 104702.
[27] J.L. Armstrong, E.D. Pylant, J.M. White, J. Vac. Sci. Technol. A 16 (1998) 123.
[28] G.T. Wang, C. Mui, C.B. Musgrave, S.F. Bent, J. Am. Chem. Soc. 124 (2002) 8990.
[29] C. Shannon, A. Campion, Surf. Sci. 227 (1990) 219.
[30] J. Eng Jr., K. Raghavachari, LM. Struck, Y.J. Chabal, B.E. Bent, G.W. Flynn, S.B. Christman, E.E. Chaban, G.P. Williams, K. Radermacher, S. Mantl, J. Chem. Phys. 106 (1997) 9889.
[31] M.P. Casaletto, R. Zanoni, M. Carbone, M.N. Piancastelli, L. Aballe, K. Weiss, K. Horn, Surf. Sci. 447 (2000) 237.
[32] M.P. Casaletto, R. Zanoni, M. Carbone, M.N. Piancastelli, L. Aballe, K. Weiss, K. Horn, Surf. Sci. 505 (2002) 251.
[33] J. Kim, K. Kim, K. Yong, J. Vac. Sci. Technol. A 20 (2002) 1582.
[34] J.W. Kim, M. Carbone, M. Tallarida, J.H. Dil, K. Horn, M.P. Casaletto, R. Flammini, M.N. Piancastelli, Surf. Sci. 559 (2004) 179.
[35] S. Tanaka, M. Onchi, M. Nishijima, J. Chem. Phys. 91 (1989) 2712.
[36] T. Bitzer, T. Alkunshalie, N.V. Richardson, Surf. Sci. 368 (1996) 202.
[37] T. Kubo, N. Minami, T. Aruga, N. Takagi, M. Nishijima, J. Phys. Chem. B 101 (1997) 7007.
[38] H. Ikeura-Sekiguchi, T. Sekiguchi, Surf. Sci. 433–435 (1999) 549.
[39] T. Bitzer, N.V. Richardson, Surf. Sci. 427–428 (1999) 369.
[40] A. Lopez, T. Bitzer, T. Heller, N.V. Richardson, Surf. Sci. 480 (2001) 65.
[41] H.-N. Hwang, J.Y. Baik, K.-S. An, S.S. Lee, Y. Kim, C.C. Hwang, B. Kim, J. Phys. Chem. B 108 (2004) 8379.
[42] H.-K. Lee, K.-J. Kim, J.-H. Han, T.-H. Kang, J.W. Chung, B. Kim, Phys. Rev. B 77 (2008) 115324.
[43] M. Ebrahimi, J.F. Rios, K.T. Leung, J. Phys. Chem. C. 113 (2009) 281.
[44] M. Ebrahimi, J.M. Chong, K.T. Leung, submitted for publication.
[45] J. Li, Y.-Q. Qu, K.-L. Han, G.-Z. He, Surf. Sci. 586 (2005) 45.
[46] X.J. Zhou, Z.H. He, K.T. Leung, Surf. Sci. 600 (2006) 468.
[47] X.J. Zhou, Q. Li, K.T. Leung, J. Phys. Chem. B 110 (2006) 5602.
[48] Q. Li, K.T. Leung, Surf. Sci. 479 (2001) 69.
[49] C.C. Cheng, J.T. Yates Jr., Phys. Rev. B 43 (1991) 4041.
[50] W. Kohn, L.J. Sham, Phys. Rev. 140 (1965) A1133.
[51] M.J. Frisch, G.W. Trucks, H.B. Schlegel, G.E. Scuseria, M.A. Robb, J.R. Cheeseman, J.A. Montgomery Jr., T. Vreven, K.N. Kudin, J.C. Burant, J.M. Millam, S.S. Iyengar, J. Tomasi, V. Barone, B. Mennucci, M. Cossi, G. Scalmani, N. Rega, G.A. Petersson, H. Nakatsuji, M. Hada, M. Ehara, K. Toyota, R. Fukuda, J. Hasegawa, M. Ishida, T. Nakajima, Y. Honda, O. Kitao, H. Nakai, M. Klene, X. Li, J.E. Knox, H.P. Hratchian, J.B. Cross, V. Bakken, C. Adamo, J. Jaramillo, R. Gomperts, R.E. Stratmann, O. Yazyev, A.J. Austin, R. Cammi, C. Pomelli, J.W. Ochterski, P.Y. Ayala, K. Morokuma, G.A. Voth, P. Salvador, J.J. Dannenberg, V.G. Zakrzewski, S. Dapprich, A.D. Daniels, M.C. Strain, O. Farkas, D.K. Malick, A.D. Rabuck, K. Raghavachari, J.B. Foresman, J.V. Ortiz, Q. Cui, A.G. Baboul, S. Clifford, J. Cioslowski, B.B. Stefanov, G. Liu, A. Liashenko, P. Piskorz, I. Komaromi, R.L. Martin, D.J. Fox, T. Keith, M.A. Al-Laham, C.Y. Peng, A. Nanayakkara, M. Challacombe, P.M.W. Gill, B. Johnson, W. Chen, M.W. Wong, C. Gonzalez, J.A. Pople, Gaussian 03, Gaussian, Inc., Wallingford, CT, 2005.
[52] A.D. Becke, J. Chem. Phys. 98 (1993) 5648.
[53] C. Lee, W. Yang, R.G. Parr, Phys. Rev. B 37 (1988) 785.
[54] NIST Mass Spec Data Center, S.E. Stein (director), in: P.J. Linstrom, W.G. Mallard (Eds.), "Mass Spectra" in NIST Chemistry WebBook, NIST Standard Reference Database Number 69, June 2005, National Institute of Standards and Technology, Gaithersburg. <http://webbook.nist.gov>.
[55] "Bond Dissociation Energies" by Y.-R. Luo, in: D.R. Lide (Ed.), CRC Handbook of Chemistry and Physics, 88th ed. (Internet Version 2008), CRC Press/Taylor and Francis, Boca Raton.